ARTICLE

Modeling Carbon Fluxes Using Multi-Temporal MODIS Imagery and CO₂ Eddy Flux Tower Data in Zoige Alpine Wetland, South-West China

Xiaoming Kang · Yanfen Wang · Huai Chen ·
Jianqing Tian · Xiaoyong Cui · Yichao Rui · Lei Zhong ·
Paul Kardol · Yanbin Hao · Xiangming Xiao

Abstract An accurate and synoptic quantification of gross primary production (GPP) in wetland ecosystems is essential for assessing carbon budgets at regional or global scales. In this study, a satellite-based Vegetation Photosynthesis Model (VPM) integrated with observed eddy tower and remote sensing data was employed and adapted to evaluate the feasibility and dependability of the model for estimating GPP in an alpine wetland, located in Zoige, Southwestern China. Eddy flux data from 2-year observations showed that temperature explained most of the seasonal variability in carbon fluxes and that warming increased GPP and ecosystem respiration, and hence affected the carbon balance of alpine wetlands. The comparison between modeled and observed GPP fluxes indicated that simulated values were largely in agreement with tower-based values ($P<0.0001$). 12-year long-term simulations (2000–2011) found that (1) there was significantly increasing trends at rate of 17.01 gCm^{-2} year^{-1} for annual GPP

($R^2=0.62$, $P=0.002$); (2) the inter-annual variation in GPP was highly sensitive to climate warming; and (3) a warmer climate can prolong the plant growing season and, by that, increase wetland productivity. Our results demonstrated that the satellite-driven VPM model has the potential to be applied at large spatial and temporal scales for scaling-up carbon fluxes of alpine wetlands.

Keywords Climate change · Remote sensing · Model · Eddy covariance · Qinghai-Tibetan Plateau · Wetland

Introduction

Terrestrial carbon (C) fluxes represent a major source of uncertainty in estimates of future atmospheric greenhouse gases accumulation and, hence, model predictions of climate

X. Kang
Chinese Academy of Forestry, Institute of Wetland Research,
Beijing 100091, China
e-mail: xmkang@ucas.ac.cn

X. Kang · Y. Wang · X. Cui · L. Zhong · Y. Hao (✉)
College of Life Sciences, University of Chinese Academy of
Sciences, Beijing 100049, China
e-mail: ybhao@ucas.ac.cn

H. Chen
Chinese Academy of Sciences, Chengdu Institute of Biology,
Chengdu 610041, China

H. Chen
College of Forestry, Northwest Agriculture and Forest University,
Yanglin 712100, China

J. Tian
State Key Laboratory of Mycology, Institute of Microbiology,
Chinese Academy of Sciences, Beijing 100101, China

Y. Rui
School of Earth and Environment, The University of Western
Australia, Crawley, WA 6009, Australia

P. Kardol
Department of Forest Ecology and Management, Swedish University
of Agricultural Sciences, 90183 Umeå, Sweden

X. Xiao
Department of Microbiology and Plant Biology, Center for Spatial
Analysis, University of Oklahoma, Norman, OK 73019, USA

change impacts on global C cycling (Friedlingstein et al. 2006; Huntingford et al. 2009). Wetlands represent one of the largest sources of this uncertainty and are regarded as one of the largest 'unknowns' regarding future C dynamics and greenhouse gas fluxes in the context of global change and climate policy-making (Sulman et al. 2009). Wetlands cover 5–8 % of the world's land surface and contain about 12 % of the global C pool, playing an important role in the global C cycle and potentially have significant impacts on the local climate (Erwin 2009; Rotenberg and Yakir 2010; Kayastha et al. 2012; Mitsch et al. 2012). Accordingly, accurate estimates of carbon dioxide (CO_2) fluxes between wetland ecosystems and the atmosphere across regions, continents and global scales are extremely valuable for precisely quantifying the global C balance and for developing accurate and predictive global C cycle models (Hao et al. 2011; Kang et al. 2011; Mitsch et al. 2012; Hao et al. 2013).

Recently, the eddy covariance (EC) technique provides continuous measurements of ecosystem-level exchanges of carbon, water, and energy at diurnal, seasonal, and inter-annual scales, allowing us to examine their changes and regulative mechanisms at multiple temporal scales (Baldocchi et al. 2001; Leuning et al. 2005; Yan et al. 2008; Kang et al. 2013). The fluxes of net ecosystem CO_2 exchange (NEE) measured with this micrometeorological method can provide valuable information related to photosynthetic period and gross primary production (GPP) at the ecosystem scale (Sanderman et al. 2003; Hao et al. 2010; Malhi 2012). However, EC method only provides very limited CO_2 flux data over footprints with restricted sizes and varied shapes (linear dimensions typically ranging from hundreds of meters to 1 km). Scaling up those CO_2 flux measurements from site level to regional or global scales is challenging because of the large spatial heterogeneity (Asner et al. 2012; Belshe et al. 2012) and interactions among ecosystems (Chen et al. 2006).

Remote sensing (RS) technology can be an effective tool for regional studies because it provides consistent and systematic observations of vegetation and ecosystems. As such, RS has become an important tool in the characterization of vegetation structure and estimation of GPP and net primary production (NPP) (Li et al. 2007; Hashimoto et al. 2012). Satellite-based model, meanwhile, is a connection of integrating EC observations and RS data for studies of regional vegetation production and C cycling. Recently, Xiao et al. (2004a, 2005a, b) have developed the satellite-based Vegetation Photosynthesis Model (VPM) that estimates GPP upon the conceptual partitioning of chlorophyll and non-photosynthetically active vegetation (NPV) within the canopy. Thorough validation of global models requires testing across a full range of biome and climate types. During the past decade, the VPM model has been further developed to include forest, agriculture and grassland ecosystems (Xiao et al. 2004a, b; Li

et al. 2007; Yan et al. 2009; Liu et al. 2012), which demonstrated its potential to scale up in situ observations of GPP from the CO_2 flux tower sites. However, so far, the VPM model has not been evaluated and applied in wetland ecosystems.

Zoige alpine wetlands, located at the eastern edge of Qinghai–Tibetan Plateau, is one of the largest alpine wetlands in the world and one of biodiversity hot-spots (Wu 1997; Chen et al. 2008). The wetland has been shown to be very sensitive to climatic changes (Chen et al. 2009), and this region is characterized by continuously increasing air temperature and declining precipitation (Tian 2005; Hao et al. 2011; Chen et al. 2013). These climate changes have the potential to significantly alter the wetland C budget. In this study, we aimed to (1) evaluate Zoige wetland vegetation through analysis of Moderate Resolution Imaging Spectroradiometer (MODIS) and C budgets with EC tower flux data in 2008–2009; (2) evaluate VPM model through CO_2 flux data measured with the EC technique in 2008 and 2009; and (3) apply VPM model to 2000–2011 period to investigate the impacts of climate change on wetland carbon uptake.

Materials and Methods

Site Description

The CO_2 eddy flux tower site was located in an alpine wetland ecosystem of the Zoige National Wetland Natural Reserve, located at the eastern edge of the Qinghai-Tibetan Plateau, Southwest China (33°56′30″N, 102°52′11″E, 3,430 m above sea level) (Fig. 1). The Zoige Plateau has an average altitude of 3,500 m, with well-developed alpine lakes and peatlands. The alpine wetlands of this region cover an area of 6,180 km^2, which is 31.5 % of the total Zoige plateau area. The region is characterized by cold Qinghai-Tibetan climatic conditions with an average annual temperature 1.6 °C and precipitation 623 mm during the period from 1990 to 2009. The warmest month is July (average: 9.3 to12.2 °C), while the coldest month is January (average: −5.8 to −11.7 °C).

At the experimental site, a typical closed organic flat wetland (a fen with a unique micro-topography, i.e., numerous scattered hummocks) was selected for this study (Fig. 1). This type of wetland represents 28 % of the total area of Zoige wetlands. Water depth at the site is on average about 5 cm, and the dry hummocks (irregularly shaped) are up to about 20 cm high above the water level. The pH of the soil slurry was 6.8–7.2. The dominant vegetation at the dry hummocks is composed of *Kobresia tibetica*, *Cremanthodium pleurocaule*, *Potentilla bifurca*, and *Pedicularis sp.*, occupying about 45 % of the whole site. *Carex muliensis* and *Eleocharis valleculosa* are the two predominant plant species scattered in hollow area.

Fig. 1 The geographical location of the Zoige alpine wetland research site. The pictures of field site, eddy tower and Meteorological Station were took in November 2008
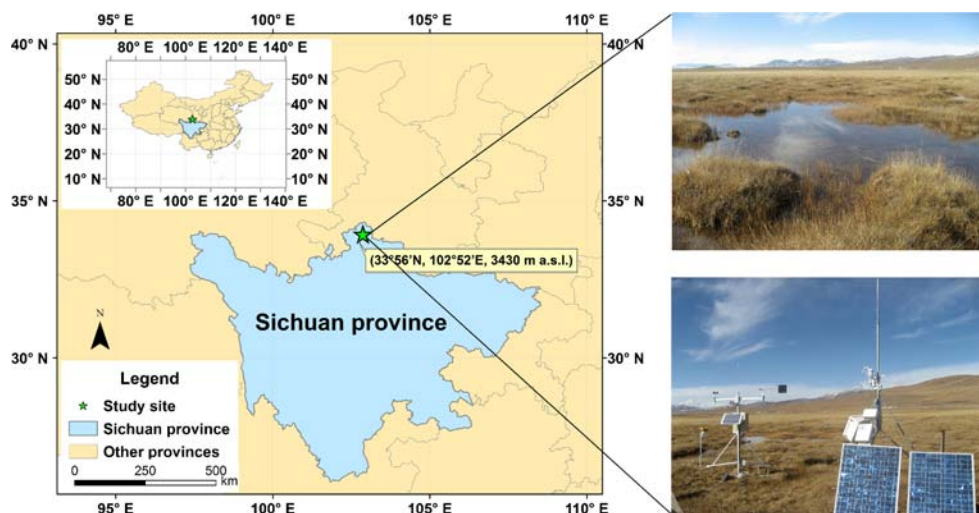
Site-Specific CO_2 Flux and Climate Data Measurements

The Eddy Covariance (EC) instrument was established at the experimental site in October 2007 (Fig. 1). Net Ecosystem CO_2 Exchange (NEE) was measured continuously with the EC system. The fetch from all directions was set to be more than 200 m based on the calculation with a footprint model (Kljun et al. 2004). Briefly, a three-axis sonic anemometer (model CSAT3, Campbell Scientific, MS, USA) with an fast response open path infrared CO_2/H_2O gas analyzer (IRGA, LI 7500, LI-COR Inc. NE, USA) was installed at a height of 2.2 m above ground level to measure the fluctuations in three wind components (w, u, v) and CO_2 fluxes. The instrument provided high frequency measurements (10 HZ), and the turbulent fluxes data were recorded as half-hour averages by a datalogger (CR5000, Campbell Scientific). In addition, some environmental factors used for gap filling calculations were also measured nearby the eddy covariance tower: net radiation and photosynthetically active radiation (PAR), air temperature and humidity, wind speed, precipitation, soil temperature and volumetric water content. All meteorological data from the sensors were collected and stored in a digital datalogger (DT80, Datataker. Australia). More details of the instrument are described by Hao et al. (2011).

Data Quality Control and GPP Estimation

Data quality control was implemented to reduce the measurement-induced uncertainties. Subsequent to data collection, half-hour average CO_2 fluxes were adjusted by the WPL (Webb, Pearman and Leuning) algorithm (Webb et al. 1980). Since low friction velocity ($u*$) and weak turbulence can result in underestimation of the CO_2 exchange rates (Goulden et al. 1996), only flux data with $u*$ greater than 0.2 m s^{-1} were used. Through screening with the data quality control process,

roughly 40 % of the data obtained from the EC tower were excluded due to the rainfall or snowfall events or the instrument malfunctions (e.g., system maintenance, power outages etc.). Gap-filling approaches such as the mean diurnal variation (MDV) (Falge et al. 2001) and the interpolation methods (Baldocchi 2003) were used to fill the data gaps. More details of the data quality control are described by Hao et al. (2011).

The CO_2 fluxes measured with the EC technique represent NEE, which is the balance between GPP and ecosystem respiration (R_e) (Law et al. 2002). So, the value of GPP can be calculated as the difference between R_e and NEE:

$$GPP = R_e - NEE \qquad (1)$$

where the positive and negative values of NEE represent net loss and net gain of carbon (CO_2 fluxes) by the soil-vegetation system, respectively.

Daily R_e is the sum of the daytime ecosystem respiration ($R_{e, day}$) and the nighttime ecosystem respiration ($R_{e, night}$):

$$R_e = R_{e,day} + R_{e,night}, \qquad (2)$$

$R_{e, night}$ is derived from the nighttime net exchange. Since the $R_{e, night}$ is related to the soil temperature, a temperature dependent model was derived from the measured nighttime average half-hour net CO_2 exchange fluxes ($R_{e, night}$):

$$R_{e,night} = a \ e^{(bTs)}, \qquad (3)$$

where Ts represents the soil temperature (°C) at the depth of 0.05 m and a (μmol of CO_2 m^{-2} s^{-1}) and b (°C) are coefficients.

Thus, by extrapolating the exponential regression correlation to the daytime periods, we estimated $R_{e, day}$ as well as GPP.

Daily GPP and climate data were then aggregated to 8-day intervals to be consistent with MODIS 8-day composites. The aggregated 8-day GPP and climate data observed in 2008 and 2009 were utilized to support model simulations and validation.

Path Analysis

To evaluate the dependence of CO_2 fluxes on several climate parameters, we used path analysis for EC data from 2008 to 2009. Path analysis has previously been applied to CO_2 fluxes data to evaluate the relative importance of various micrometeorological factors in regard to seasonal and annual CO_2 fluxes variability (Saito et al. 2008; Wang et al. 2011; Matías et al. 2012). Path analysis is an extension of multiple regressions and can be used to provide estimates of the magnitude and significance of hypothesized causal connections among variables. In this study, we focused on the following five environmental variables: air temperature (Ta), Ts, PAR, precipitation (PPT) and soil water content (SWC) at a depth between 0 and 5 cm and its importance in long-term CO_2 fluxes change of Zoige alpine wetland ecosystem. We tested the relationships among variables and depicted mediated and nonmediated relationships in the model. The model was drawn using observed variables and was recursive. Bootstrapping was used to determine the significance of the mediated relationships. Goodness-of-fit indices were used to evaluate the model. The degree of fit between the covariance in the observed data with that expected if the working model is true was first examined by a goodness-of-fit chi-square (x^2). Non-significant x^2 indicates that the pattern of covariance predicted by the hypothesis is no different from observed data, and thus the model could be accepted. In addition, the normed fit index (NFI) and the comparative fit index (CFI) were used, as they are not affected by the number of subjects and the estimation method, respectively. NFI and CFI range between 0 and 1, and values greater than 0.9 indicate a good fit of the model to the data. SPSS was used in all analyses with alpha levels of 0.05. We performed path analysis by using AMOS 20.0 (Analysis of Moment Structures).

MODIS Imagery

The time series data of site-specific vegetation indices during 2000–2011 were extracted from one MODIS pixel that was centered on the targeted EC tower. The MODIS Land Science Team provides several data products derived from MODIS observations to the public, including the 8-day composite Land Surface Reflectance (MOD09A1). We downloaded the 8-day composite MOD09A1 datasets from the Oak Ridge National Laboratory's Distributed Active Archive Center (DAAC) website (http://daac.ornl.gov/MODIS/modis.shtml). The datasets include seven spectral bands at a spatial resolution of 500 m, and have been corrected for the effects of atmospheric gases, aerosols, and thin cirrus clouds. Then, reflectance values of four spectral bands (blue band (459–479 nm), red band (620–670 nm), near infrared (NIR) band (841–876 nm), shortwave infrared (SWIR) band (1,628–1,652 nm)) over 2004–2007 were used to calculate three

site-specific vegetation indices: Normalized Difference Vegetation Index (NDVI) (Tucker 1979), Enhanced Vegetation Index (EVI) (Huete et al. 1997), and Land Surface Water Index (LSWI) (Xiao et al. 2004a).

NDVI is an operational, global-based vegetation index and has been widely used in describing terrestrial vegetation. However, the open loop structure (no feedback) of the NDVI equation renders it still susceptible to large sources of error and uncertainty over variable atmospheric and canopy background conditions.

$$NDVI = \frac{\rho_{nir} - \rho_{red}}{\rho_{nir} + \rho_{red}} \tag{4}$$

where ρ_{nir} and ρ_{red} are the reflectance of NIR and red bands, respectively.

Owing to these defects of the NDVI, the EVI was proposed based on a feedback-based approach that incorporates both background adjustment and atmospheric resistance concepts into the NDVI.

$$EVI = 2.5 \times \frac{\rho_{nir} - \rho_{red}}{\rho_{nir} + (6 \times \rho_{red} - 7.5 \times \rho_{blue}) + 1} \tag{5}$$

where ρ_{nir}, ρ_{red} and ρ_{blue} are the reflectance of NIR, red and blue bands, respectively.

The SWIR spectral band is sensitive to vegetation water content and soil moisture. Hence the water-sensitive LSWI was calculated as the normalized difference between NIR and SWIR spectral bands (Xiao et al. 2004a):

$$LSWI = \frac{\rho_{nir} - \rho_{swir}}{\rho_{nir} + \rho_{swir}} \tag{6}$$

where ρ_{nir} and ρ_{swir} are the reflectance of NIR and SWIR bands, respectively.

Description of the VPM Model

The VPM is built upon the conceptual partitioning of chlorophyll ($FPAR_{chl}$) and non-photosynthetically active vegetation (NPV) within the canopy, and it estimates GPP over the photosynthetically active period of vegetation (Xiao et al. 2004a). GPP is estimated using the following function:

$$GPP = \varepsilon_g \times FPAR_{chl} \times PAR \tag{7}$$

where ε_g is the light use efficiency (μmol CO_2/μmol photosynthetic photon flux density, PPFD), PAR is the photosynthetically active radiation (μmol PPFD), and $FPAR_{chl}$ is the fraction of PAR absorbed by leaf chlorophyll in the canopy. $FPAR_{chl}$ is calculated as:

$$FPAR_{chl} = \alpha \times EVI \tag{8}$$

where EVI is the Enhanced Vegetation Index, α is the coefficient in the EVI-$FPAR_{chl}$ linear function, which is set to be 1.0.

The parameter ε_g is affected by temperature, water and leaf phenology:

$$\varepsilon_g = \varepsilon_0 \times T_{\text{scalar}} \times W_{\text{scalar}} \times P_{\text{scalar}} \qquad (9)$$

where ε_0 is the maximum light use efficiency (LUE) (μmol CO_2/μmol PPFD), and T_{scalar}, W_{scalar}, and P_{scalar} are the down-regulation scalars for the effects of temperature, water and leaf phenology on LUE, respectively. In the VPM model, ε_0 is estimated for each type of ecosystem individually. In order to obtain the ε_0 values for alpine wetland, we had estimated the nonlinear model between NEE and PAR by using the Michaelis–Menten function (Eq. (4)), based on data collected during the peak period of vegetation growth (from May to September) in 2008 and 2009. Here, we used 0.53 μmol CO_2/ μmol PPFD as ε_0 for 2008 and 2009, respectively:

$$NEE = \frac{\varepsilon_0 \times PAR \times GPP_{\max}}{\varepsilon_0 \times PAR \times GPP_{\max}} - R_{eco} \qquad (10)$$

where the $GPP_{\max}$ (mg CO_2 m^{-2} s^{-1}) is the ecosystem maximum photosynthetic capacity, and R_{eco} is ecosystem respiration. The estimated ε_0 value is used as an estimate of the maximum light use efficiency parameter in the VPM model.

T_{scalar} was estimated at each time step using the following equation:

$$T_{scalar} = \frac{(T - T_{\min})(T - T_{\max})}{[(T - T_{\min})(T - T_{\max})] - (T - T_{opt})^2} \qquad (11)$$

where $T_{\min}$, $T_{\max}$ and T_{opt} are minimum, maximum and optimal temperature for photosynthetic activities, respectively.

W_{scalar} was calculated by utilizing an alternative and simple approach using a water-sensitive vegetation index:

$$W_{scalar} = \frac{1 + LSWI}{1 + LSWI_{\max}} \qquad (12)$$

where $LSWI_{\max}$ is the maximum LSWI (Land Surface Water Index) during the study period. As a parameter describing water status, $LSWI_{\max}$ varies across years. We chose the maximum LSWI values during the plant growing season for each year as $LSWI_{\max}$. The $LSWI_{\max}$ value is 0.26 and 0.36 for 2008 and 2009, respectively.

P_{scalar} is included to account for the effect of leaf age on photosynthesis at the canopy level, and depends on leaf longevity:

$$P_{scalar} = \frac{1 + LSWI}{2} \qquad (13)$$

In this study, since this was the first time for VPM to be applied for C studies for the alpine wetland in China, we first tested VPM against part of observed data for calibration. In alpine ecosystems, temperature is often the major environmental variable constraining CO_2 fluxes. Therefore, the calibration focused on three groups of temperature input parameters for plant growth, such as $T_{\min}$, $T_{\max}$ and T_{opt}. The temperature parameters for the alpine wetland simulated in the study were carefully calibrated based on the long term observed datasets of the local air temperature data and observed GPP data to ensure they could correctly represent the local vegetation community. When air temperature falls below T_{min}, T_{scalar} is set to zero. In this study, we finally used $T_{\min}$ of 0 °C, T_{opt} of 16 °C and $T_{\max}$ of 32 °C for Zoige wetland to support VPM simulation.

By running the VPM model at a 8-day time scale with vegetation indices derived from the 8-day MODIS surface reflectance product and site-specific data of air temperature and PAR, we obtained the seasonal and annual dynamics of GPP for each year (2008 and 2009). The simulated GPP data from the VPM model were then compared with the observed GPP data from the EC tower for 8-day intervals to validate the applicability of the VPM model to the Zoige alpine wetland.

Statistics for Comparison Between VPM-Predicted and Tower-Based GPP Fluxes

As suggested by Addiscott and Whitmore (1987) and Smith et al. (1997), to quantify the discrepancy between the simulated and observed results, we adopted three statistical criteria for the validation tests: the coefficient of determination (R^2, Eq. (14)), the root of mean square error (RMSE, Eq. (15)) and the relative mean deviation (RMD, Eq. (16)). Each criterion investigates a specific aspect of the correlation. The R^2 represents a common regression coefficient indicating the ability of the model to explain variation in the observed values and to assess how well the shape of the simulation matches that of the measured data (Janssen and Heuberger 1995). The RMSE provides the model's prediction error by heavily weighting high errors, whereas the RMD weights all errors the same, which tends to smooth out the discrepancies between modeled and observed values. The values of RMD close to 0 indicate the absence of bias in the model (Huang et al. 2009). All statistical calculations were performed using SPSS version 20.0 (SPSS Inc., Chicago/United States).

$$R^2 = \left(\frac{\sum \left(O_i - \overline{O}\right)\left(P_i - \overline{P}\right)}{\sqrt{\sum \left(O_i - \overline{O}\right)^2 \sum \left(P_i - \overline{P}\right)^2}} \right)^2 \qquad (14)$$

$$RMSE = \sqrt{\frac{\sum_{i=1}^{n}(P_i - O_i)^2}{n}} \qquad (15)$$

$$RMD = \frac{100}{\overline{O}} \sum_{i=1}^{n} \frac{P_i - O_i}{n} \qquad (16)$$

where O_i and P_i represent the observed and model-predicted values, respectively. $\overline{O}$ and $\overline{P}$ are the mean of the observed and predicted values, respectively. n is the number of observations.

Results

Seasonal Dynamics of Observed Climate and CO₂ Flux in 2008–2009

There was pronounced seasonal variation in mean 8-day Ta, ranging from −12.9 to 12.4 °C (Fig. 2a). PAR was somewhat lower in 2008 than that in 2009; in both years values were markedly lower in winter than in summer. The annual mean Ta in 2008 was 1.5 °C lower than the long-term (1990–2009) mean (1.6 °C); whereas the respective value in 2009 was 2.6 °C higher than the long-term mean. Moreover, patterns of precipitation (PPT) differed between years

(Fig. 2b, c). Long-term climate data in the region of the study site reveals that the annual precipitation (rainfall and snowfall) in 2008 was 465 mm lower than the long-term mean (623 mm); whereas the respective value in 2009 was 596 mm also lower than the long-term mean.

The aggregated 8-day observed NEE, GPP and R_e time series derived from the EC flux tower showed large seasonal and inter-annual variation (Fig. 3a). The seasonal dynamics of CO₂ fluxes could be explained in part by the seasonal dynamics of Ta and PAR (Figs. 2a and 3). During the dormant period (from November to April), characterized by low air temperature and frozen soils inhibiting photosynthetic activity, GPP values were near zero, and NEE values were low and largely driven by ecosystem respiration (Fig. 3a). After this period, the ecosystem photosynthesis capability gradually increased as PAR intensified and air temperature crossed the limit of minimum temperature of photosynthetic activities. GPP started to increase in early May or late April, and ended in

Fig. 2 Seasonal dynamics of (**a**) mean 8-day air temperature (Ta) and photosynthetically active radiation (PAR), (**b**) aggregated 8-day precipitation, and (**c**) aggregated monthly precipitation in 2008 and 2009 and long-term means for 1990–2009
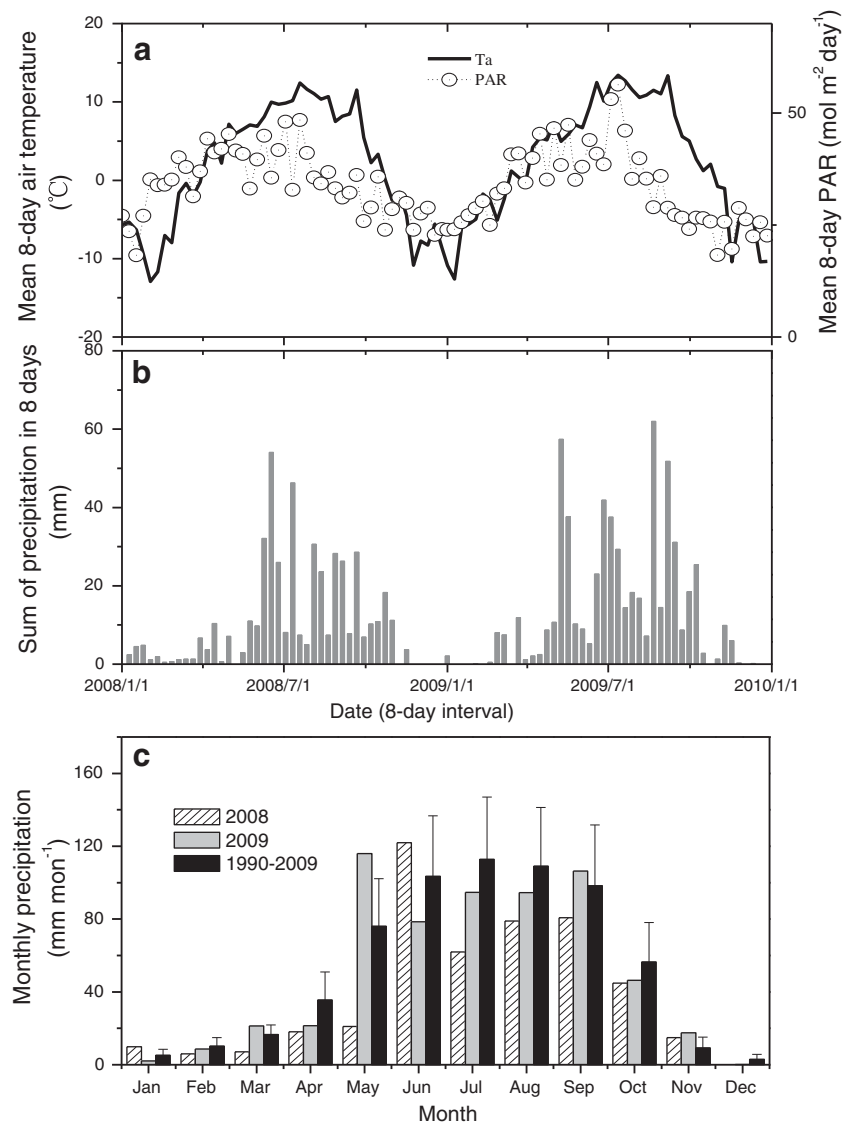
late October in both years. The plant growing season in 2008 and 2009, defined as the carbon uptake period, was from early May to late October and from late April to late October, respectively. GPP and R_e gradually increased and reached peak values in July or August. Thereafter, GPP and R_e gradually decreased as soil temperature decreased and vegetation started to senesce. The duration of net CO_2 uptake (NEE < 0) in 2009 (128 days) was slightly longer than in 2008 (120 days). These results implied that temperature played an important role in determining the seasonal variation of CO_2 fluxes (Fig. 3b–d). At the annual scale, the Zoige wetland ecosystem was a sink of atmospheric CO_2 with 47.1 and 79.7 g C m^{-2} year^{-1} sequestered in 2008 and 2009 based on the observed data, respectively. The results implied that the Zoige wetland was a sink of atmospheric CO_2 both in 2008 and 2009 although the droughts in both years substantially enhanced the C losses from the ecosystem.

Determinants of CO_2 Fluxes

Goodness-of-fit indices (x^2, NFI and CFI) indicate a good fit of the model to the data (Fig. 4). Among the five factors (Ta, Ts, SWC, PAR, and PPT) directly affecting CO_2 fluxes during the growing season, the path coefficients of Ts and SWC were 0.65 and −0.42 for GPP ($P<0.001$; Fig. 4a), 0.41 ($P<0.05$) and −0.11 ($P>0.05$) for R_e (Fig. 4b), −0.74 and 0.49 for NEE ($P<0.01$; Fig. 4c), respectively–much higher than the

contributions of the other environmental factors. Furthermore, the total causal effect (the sum of the direct and indirect effects) of Ta on CO_2 fluxes was 0.59 for GPP, 0.71 for R_e and −0.31 for NEE. Additionally, soil water content explained a significant part of the variation for GPP and NEE, but not for R_e (Fig. 4).

Seasonal Dynamics of Vegetation Indices

The EVI and NDVI indices shows that the plant growing season for this wetland site is from early May and late April to late October in 2008 and 2009, respectively, reaching a plateau value during late summer (early July) to early autumn (late August), then starting to decline again (Fig. 5a). However, seasonal dynamics of the EVI differed from those of the NDVI in terms of phase and magnitude. The NDVI remained at peak values for a longer time than the EVI. Further, the peak EVI values were 0.57 and 0.65 for 2008 and 2009, respectively, while the peak NDVI values were 0.78 and 0.83. The seasonal dynamics of EVI and NDVI could be explained in part by the seasonal dynamics of air temperature (Fig. 5b–c) and PAR (Fig. 2a). The LSWI also showed seasonal dynamics, but less than the NDVI and EVI, especially during the growing season. The peak LSWI values were 0.26 (DOY 177) and 0.34 (DOY 193) for 2008 and 2009, respectively; this may indicate that inter-annual changes of LSWI values reflect the precipitation differences between 2008 (465 mm) and
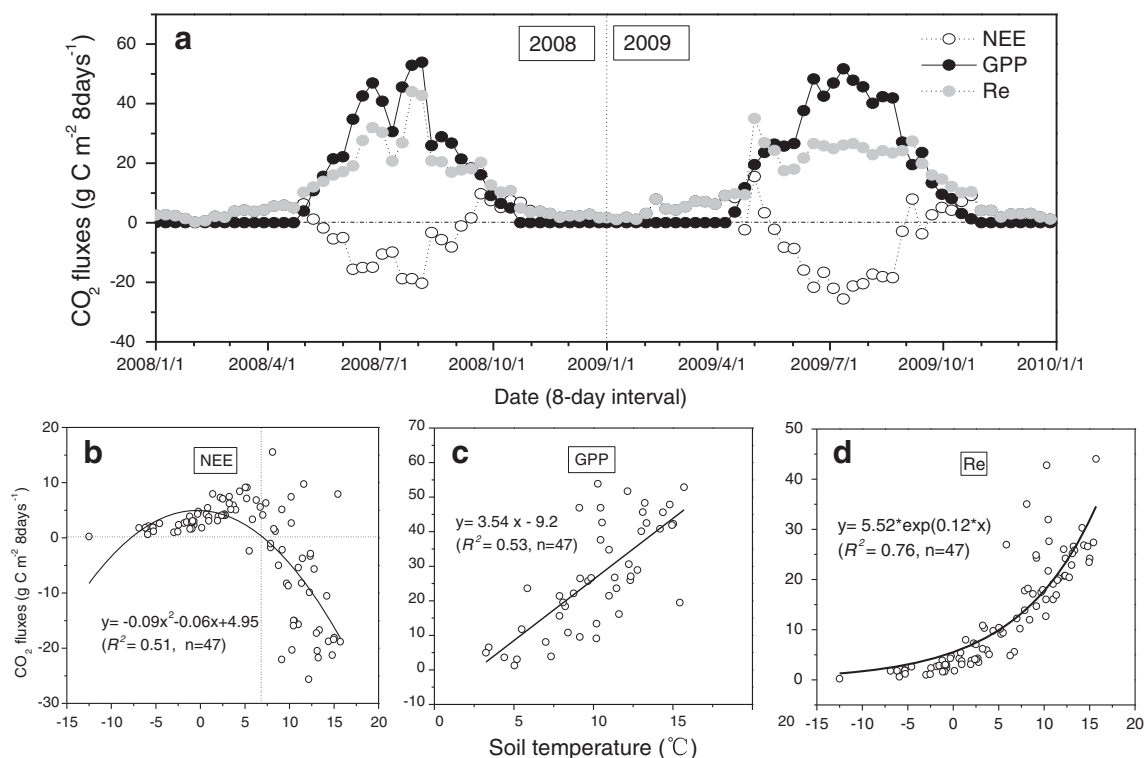
Fig. 3 **a** Seasonal dynamics of aggregated 8-day net ecosystem CO_2 exchange (NEE), gross primary production (GPP) and ecosystem respiration (R_e), and the relationship between soil temperature and **b** NEE, **c** GPP, **d** R_e during 2008–2009 in Zoige alpine wetland
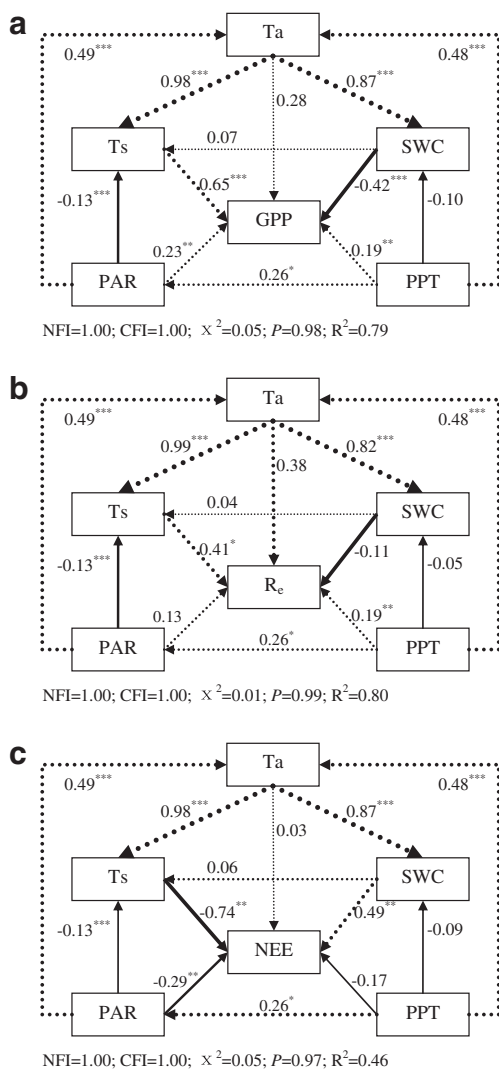
Fig. 4 Path diagrams illustrating the effects of environmental variables (air temperature (Ta), soil temperature at a depth of 5 cm (Ts), photosynthetically active radiation (PAR), soil water content (SWC), and precipitation (PPT)) on gross primary production (GPP), ecosystem respiration (R_e) and net ecosystem CO_2 exchange (NEE) during 2008–2009. The thickness of each *arrow* and the values besides the *arrows* represent the path coefficients, both with the standardized regression weights obtained from the model indicated. *Solid arrows* represent negative correlations, and *dashed* ones are positive correlations. All the variables used in the analyses are 8-day aggregated values. Fit statistics (*NFI* normal fit index; *CFI* comparative fit index; *P* value; x^2, chi-square; R^2, squared multiple correlation) are given at the bottom of each panel. *$p < 0.05$; **$p < 0.01$; ***$p < 0.001$

2009 (596 mm). During dormant period, the LSWI values were generally low, often below zero. Low LSWI in the dormant period reflects the low precipitation and may indicate some degree of water stress (Fig. 2b–c). The rapid decline of both the EVI and LSWI in October indicates early plant senescence, while high EVI and LSWI values in July indicate a rapidly developing and photosynthetically active canopy in responses to warmer and wetter conditions (Fig. 5a).

Relationships Between Vegetation Indices and Observed GPP

The seasonal dynamics of GPP correlated well with the dynamics of the vegetation indices (EVI, NDVI, and LSWI) (Figs. 5a and 6). The quantitative relationships between the vegetation indices and CO_2 flux data clearly demonstrated that the EVI ($R^2 = 0.62$, $P < 0.001$) had a higher predictive power in terms of the phase and magnitude of photosynthesis than the NDVI ($R^2 = 0.49$, $P < 0.001$) for the Zoige wetland ecosystem (Fig. 6a, b). Moreover, the regression of LSWI against observed GPP values ($R^2 = 0.64$, $P < 0.001$; Fig. 6c) showed that land surface water content was significantly correlated with carbon fluxes measured at the EC tower.

## VPM Simulations Against Observations in 2008 and 2009

Patterns and magnitudes of the simulated GPP were well in agreement with the observation, accurately simulating the trajectories of the observed seasonal and inter-annual variation in GPP (Fig. 7a). The VPM model also accurately captured the U pattern of the plant growth driven by the variation in temperature and PAR. For both years, linear regression analysis of the modeled and observed GPP and three statistical criteria for the validation tests showed a strong correlations between our simulation and observations ($P < 0.0001$; Fig. 7b–d; Table 1). Moreover, Statistical analysis of the residual values of GPP showed that the residuals were not randomly distributed (Fig. 7e). In absolute magnitude, low residual values of GPP were generally associated with low prediction errors of model, whereas high GPP residual values were associated with high prediction errors of model. At the annual scale, the modeled GPP values were only slightly higher than the observed GPP values in 2008, and only slightly lower than the observed GPP in 2009, with relative error (RE) values of 2 % and −6 %, respectively (Table 2). Furthermore, averaged GPP predicted for the 2 years of study agreed reasonably well with the observed values, with −2 % mean RE (Table 2).

Inter-Annual Variation of GPP in 2000–2011 as Predicted by the VPM Model

Given the encouraging results from the model validation tests, we utilized the VPM model for estimating and reproducing long-term seasonal and inter-annual GPP dynamics for the tested Zoige alpine wetland. We built a 12-year (2000–2011) daily weather dataset (air temperature, precipitation and PAR) obtained from the climate database of our local meteorological station and the studied station of China Meteorological Administration and we obtained the time-series dataset of vegetation indices derived from satellite images for the very location. By running the VPM model for this 12-year baseline climate scenario, we obtained seasonal and annual GPP

Fig. 5 **a** Seasonal dynamics of vegetation indices (*NDVI* normalized difference vegetation index; *EVI* enhanced vegetation index; *LSWI* land surface water index), and linear regression analyses between air temperature and **b** NDVI, **c** EVI during 2008–2009 in Zoige alpine wetland
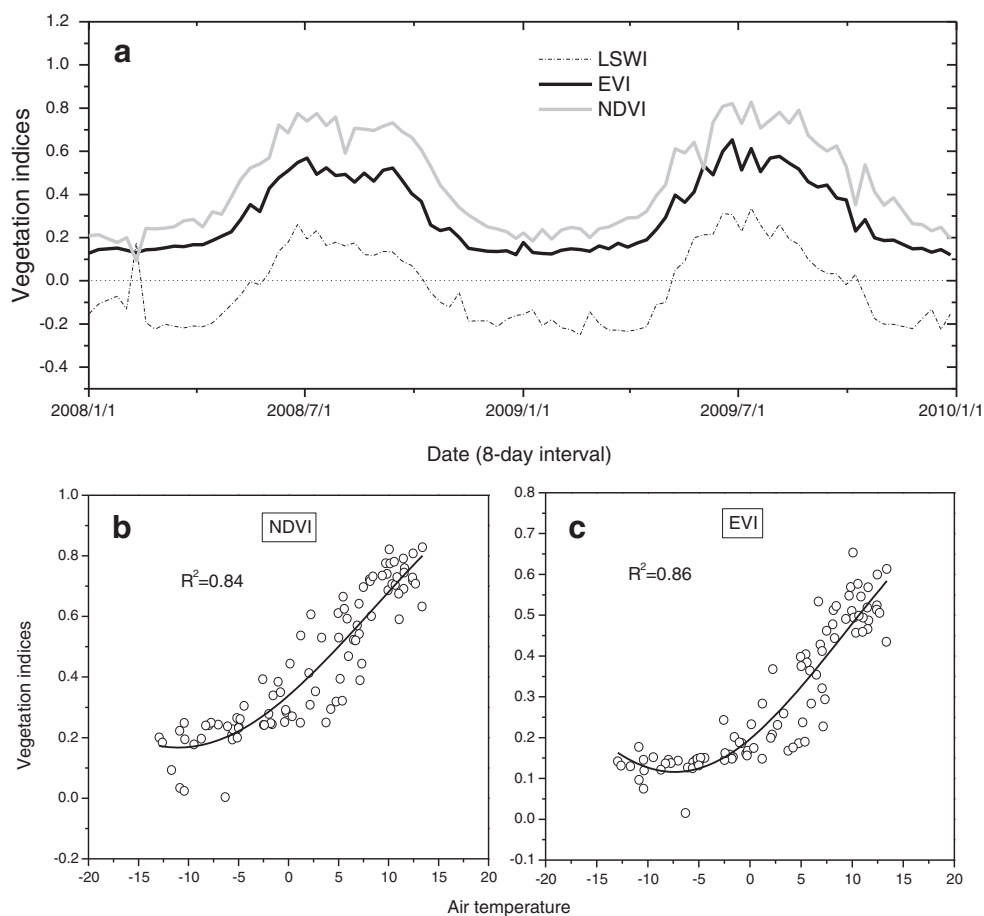

dynamics for each year. There were strong and positive exponential relationships between air temperature and the vegetation indices EVI and NDVI (Fig. 8a, b). The annual GPP over 12 years varied between 485 and 720 g C m^{-2} year^{-1} (Fig. 8c) and was mainly driven by inter-annual variation in air temperature (Fig. 9). We also detected a significantly increasing trend of annual GPP (R^2=0.46, P=0.02) and oscillation frequency over the course of the experiment. Correspondingly, we also found that the average annual air temperature at the study site increased during this period.

Discussion

Effects of Weather Conditions on CO$_2$ Flux

Various environmental factors directly and indirectly affect CO$_2$ fluxes (GPP, R$_e$ and NEE) (Hao et al. 2011; Kang et al. 2011; Matías et al. 2012; Hao et al. 2013; Kang et al. 2013). In this study, we used a simple path analysis to examine the relative causality of these environmental variables in controlling CO$_2$ fluxes (see Fig. 4). The results indicate that soil
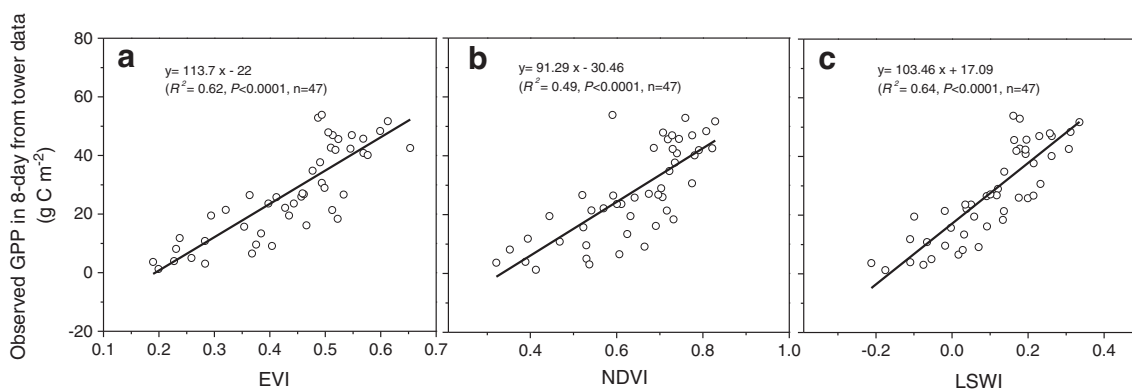
Fig. 6 Linear regressions between 8-day (**a**) EVI, (**b**) NDVI, (**c**) LSWI and gross primary production (GPP) during 2008–2009 in Zoige alpine wetland

Fig. 7 **a** Comparisons between aggregated 8-day simulated and observed gross primary production (GPP); **b**–**e** Simulated vs. observed 8-day GPP and scatter plot of simulated 8-day GPP vs. residuals (observed– simulated) for Zoige alpine wetland in 2008 and 2009. *Dashed line* is 1:1
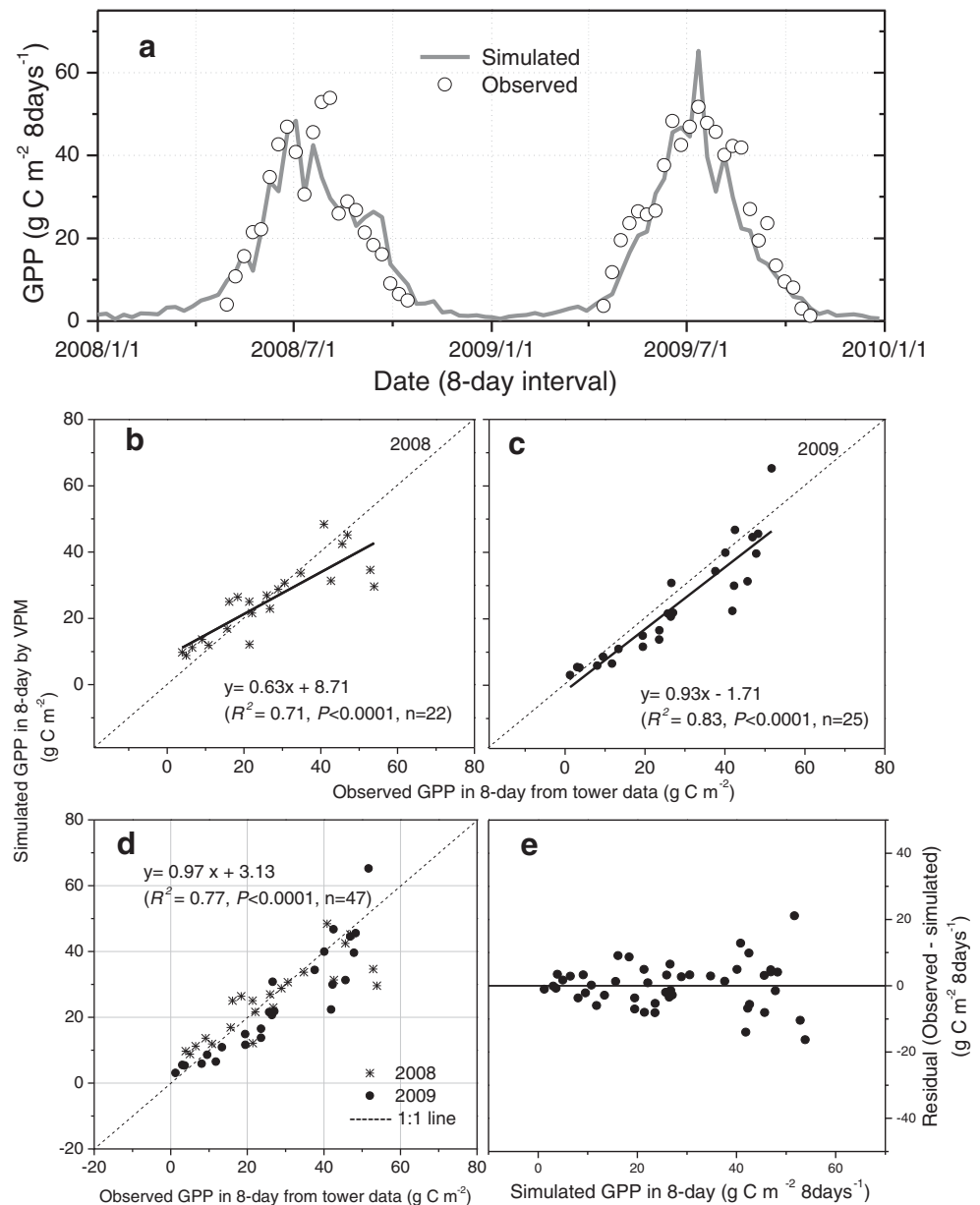
temperature had the strongest effects on GPP, R_e, and NEE fluxes, which explained most of the seasonal variability in CO_2 fluxes, consistent with the large seasonal temperature variation on this high altitude alpine wetland. The path analysis also showed that soil temperature was strongly affected by air temperature. Taken together, these results indicate that the C cycling of alpine wetlands is strongly temperature-driven. To note, at high altitudes, the seasonal variation in temperature is high. In alpine ecosystems, low temperature is often the major environmental variable constraining CO_2

Table 1 Comparisons of observed and simulated 8-day GPP during 2008–2009 in Zoige alpine wetland

Observed vs simulated	Year	R^2	RMSE (%)	RMD (%)	n
8-day GPP	2008	0.56[***]	11.97	−7.62	22
	2009	0.83[***]	7.51	−13.72	25
	2008–2009	0.68[***]	9.85	−21.33	47

R^2, the coefficient of determination; *RMSE* the root of mean square error; *RMD* the relative mean deviation

[***]Significant at probability levels of 0.0001

Table 2 Environmental conditions and comparisons between the observed and simulated annual GPP accumulated from 8-day observations and simulations during 2008–2009 in Zoige alpine wetland

Year	Temperature (°C)	PAR[a] (mol m^{-2})	Precipitation (mm)	GPP$_{obs}$[a] (g C m^{-2})	GPP$_{vpm}$[a] (g C m^{-2})	RE[a] (g C m^{-2})
2008	1.58	1521	465	607.76	620.86	2 %
2009	2.55	1572	596	672.1	634.25	−6 %
Mean (2008–2009)	2.07	1547	531	639.93	627.56	−2 %

[a] Abbreviations: *GPP* gross primary production; *PAR* photosynthetically active radiation; *GPP$_{obs}$*, observed GPP in 8-day from FLUX tower data; *GPP$_{vpm}$*, simulated GPP in 8-day by VPM; *RE* (relative error) = [(GPP$_{VPM}$−GPP$_{obs}$)/GPP$_{obs}$] × 100 %

fluxes (Huxman et al. 2003; Hao et al. 2011). Previous studies of the same alpine wetland have pointed out the importance of temperature in controlling C fluxes (e.g. Inglett et al. 2012; Schedlbauer et al. 2012; Xie et al. 2013), and soil temperature and moisture have also been shown to be important factors controlling CO_2 fluxes in other ecosystems, such as, for example, semi-arid grasslands in Inner Mongolia, China (Wang et al. 2011). However, these previous studies did not compare the relative importance and contribution of other environmental factors affecting CO_2 fluxes. As such our path analyses provide important new information, clearly demonstrating that the temperature–both air and soil temperature–was the main affecting factor for CO_2 fluxes over a 2-year period and a 12-year period this high altitude alpine wetland. Our findings imply that if global temperatures continue to

increase in the (near) future, the Zoige alpine wetland is likely to uptake more carbon from atmosphere.

Wetland Vegetation and Phenology as Observed by Satellite and CO_2 Flux Tower

Vegetation indices obtained from MODIS data provide valuable information into the processes (e.g., growing season length and water status) that regulated ecosystem carbon budgets and an indirect approach for predicting GPP (Guindin-Garcia et al. 2012). Note that both EVI and NDVI started to increase in late April to early May, corresponding well with the increase of GPP in early May. Evidently, one can use those dates with consistent increases of vegetation indices (NDVI, EVI and LSWI) in spring after snowmelt as the starting

Fig. 8 The relationship between air temperature (Ta) and (**a**) EVI, (**b**) NDVI; and (**c**) the long-term dynamics of aggregated 8-day GPP and annual GPP simulated by the VPM model for Zoige alpine wetland
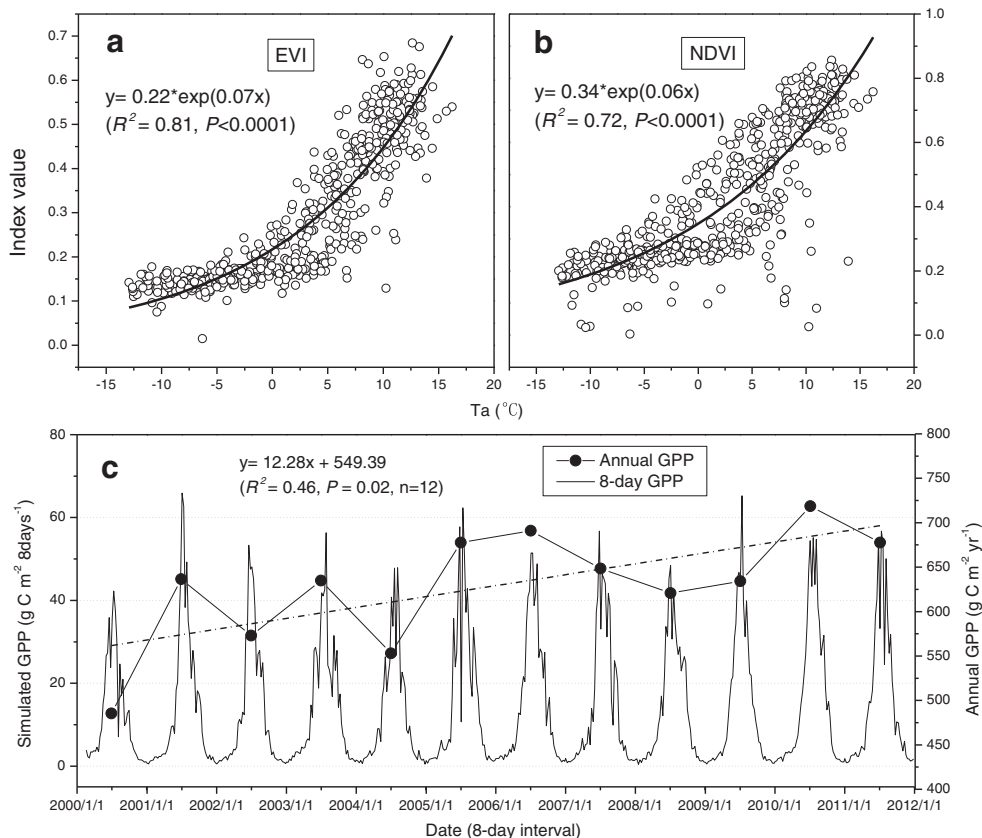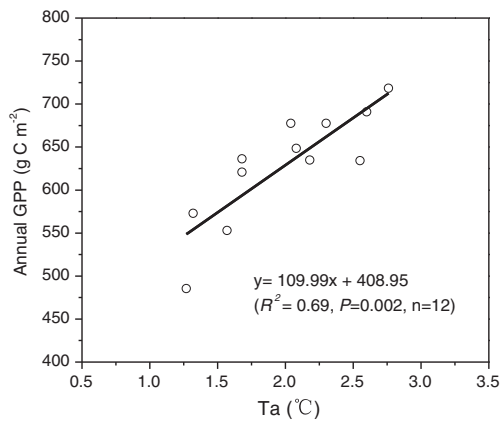
Fig. 9 The relationship between annual GPP simulated by VPM and observed mean air temperature (Ta) during 2000–2011 in Zoige alpine wetland

date of the plant growing season. LSWI values reached its lowest value in late October, corresponding well with the ending dates of the carbon uptake period. While one can still use a threshold of NDVI or EVI to define the ending date of the plant growing season, LSWI seems to offer a clean and simple alternative approach to delineate the ending dates of the plant growing season for Zoige wetlands. Moreover, the EVI is an 'enhanced version' of the NDVI and was developed to optimize the vegetation signal with improved sensitivity in high biomass regions, while correcting for canopy background signals and reducing atmosphere influences (Li et al. 2007; Mu et al. 2007). In this study, regression analyses between the vegetation indices and observed GPP (see Fig. 6) indicated that for our alpine wetland ecosystem the EVI better correlated with the seasonal dynamics of GPP, and hence, has more biological significance in GPP predictions than the NDVI.

VPM Model Simulation

Comparisons between simulated and observed GPP results showed that the EVI-based VPM model can capture the overall trends of the Zoige alpine wetland phenology and provides an accurate estimation of GPP ($R^2=0.77$). These results as well as results from earlier VPM studies (Xiao et al. 2004a; Li et al. 2007; Wu et al. 2008; Yan et al. 2009; Liu et al. 2012) indirectly support the chlorophyll-$FPAR_{chl}$-EVI hypotheses and leaf water-LSWI hypothesis as implemented in the VPM model, and demonstrate the potential of the satellite-driven VPM model for scaling up GPP measured at CO_2 flux tower sites to much larger spatial scales, which is an important issue for the study of C cycling and sequestration at regional and global scales.

In addition, compared with other model (such as MODIS-PSN), VPM works much better. We downloaded the 8-day composite GPP products (MOD17A2) data sets from the Oak Ridge National Laboratory's Distributed Active Archive Center (DAAC) website (http://daac.ornl.gov/MODIS/modis.shtml) to get GPP results from MODIS-PSN during 2008–2009 (see Fig. 10). Clearly, the predicted GPP from MODIS-PSN underestimated GPP relative to that observed from EC tower and that simulated by VPM model during the rapid growth and peak growth stage, which might be attributed to several reasons that may explain the discrepancy between the $GPP_{MOD17A2}$ and GPP_{obs}. One is that $GPP_{MOD17A2}$ uses global climate dataset, there is a possibility that climate data from the global climate dataset do not match the local climate data. Second, it could be light use efficiency parameter (ε_g) and the over-correction of vapor pressure deficit (VPD) on light use efficiency (LUE) in MODIS-PSN (Goetz et al. 1999; Wu et al. 2008). ε_g is the basis and one of key steps for using the
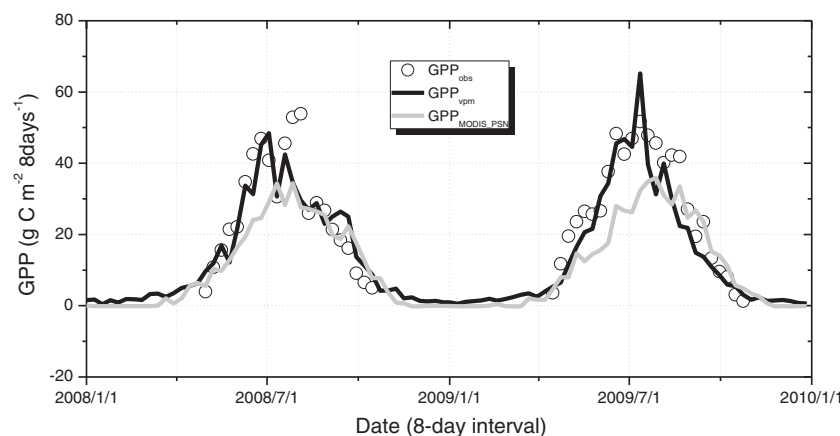
Fig. 10 A comparison between observed 8-day GPP from flux tower (GPP_{obs}) and predicted GPP from VPM (GPP_{VPM}) and MODIS-PSN ($GPP_{MODIS-PSN}$) in 2008 and 2009. GPP from MODIS-PSN was clearly underestimated during the rapid growth and peak growth stage. VPM accurately simulated the trajectories of the observed seasonal and inter-annual variation in GPP. The MODIS-PSN algorithm (Running et al. 1999; Turner et al. 2003) is used to generate the standard MODIS GPP/NPP product (MOD17A2), which is now available to the public (http://www.edc.usgs.gov)

Production Efficiency Models to estimate GPP (Running et al. 1999). If ε_g differs significantly among vegetation types, these differences should be accounted for when estimating GPP with remotely sensed data. Therefore, the eddy covariance technique provides a significant potential approach to estimate the canopy-level ε_g (Turner et al. 2003) and the comparison indicates that $GPP_{MOD17A2}$ is substantially different from the in-situ data, which calls for a caution in using $GPP_{MOD17A2}$ for regional analysis in wetlands.

Estimating Long-Term GPP Dynamics

Long-term GPP simulation (2000–2011) further suggests an important role of temperature in long-term GPP dynamics, and indicates the potential of further increase in C sequestration under predicted scenario of global warming. The results from our modeling study indicate that when the climate becomes warmer, the plant growing season extends, and hence, wetland production increases. The overall increase in the VPM-modeled GPP between 2000 and 2011 is in agreement with expectations for high-latitude ecosystems under global warming (e.g. Oechel et al. 2000; Tagesson et al. 2012). Warming directly affects plant growth and shifts in plant species across a range of tundra ecosystems (Walker et al. 2006; Elmendorf et al. 2012). Several studies indicate that plant aboveground net primary production (ANPP) has variable responses to warming in arctic and alpine regions, with reported increases, decreases, or no change (Houborg and Soegaard 2004; Wan et al. 2005; Klein et al. 2007; Post and Pedersen 2008). Wania et al. (2009) modeled strong increases in Arctic annual NPP using a dynamic global vegetation model (DGVM). In their case, the NPP trend was also related to strong sensitivity to changes in air temperature. Similarly, through a controlled asymmetrical warming (1.2/1.78C during daytime/nighttime) experiment from 2006 to 2010 in an alpine meadow, Wang et al. (2012) found that warming stimulated ANPP and significantly increased the coverage and height of a dominant species and graminoid coverage in the community increased, and these changes explained 32 % and 18 % of the variation in annual ANPP during the 5-year experimental periods. Furthermore, a meta-analysis of 20 warming experiments demonstrated an average of 19 % increase in aboveground plant productivity under warming in comparison to that under control (Rustad et al. 2001).

In addition to GPP, ecosystem respiration was also affected by warming (Hao et al. 2013). The balance of these two major carbon fluxes determines whether terrestrial ecosystems will act as a net C sink or source under climate changes (Kang et al. 2011). In this study, however, we only focused on the effects of warming on wetland productivity. So, future studies on the C balance of the Zoige wetland should integrating continuous EC measurement data and RS data over longer time periods with ecological model to evaluate whether warming will increase C emissions and if increased emission will exceed the increased amount of C uptake.

Model Uncertainty

We showed that there was good agreement between observed (GPP_{obs}) and simulated (GPP_{sim}) values of gross primary production for the photosynthetically active period during 2008–2009 in the targeted wetland. However, there were some differences between GPP_{sim} and GPP_{obs}, such as lower GPP_{sim} in late July and early August in 2008, and higher GPP_{sim} in late August in 2009. Discrepancies between GPP_{obs} and GPP_{sim} may be attributed to three sources of errors. The first source is the sensitivity of the VPM model to PAR and precipitation. In some cases, under/over-estimation of GPP is attributed to lower/higher input PAR values for the assumed linear relationship between GPP and PAR in VPM model (Zhang et al. 2009). For further applications of the VPM model at large spatial scales, PAR is the most critical variable in the estimation of the seasonal dynamics of GPP_{sim}, but it varies substantially over space and time (Xiao et al. 2004b). Therefore, improvement in measurement of PAR (both direct and diffusive) at large spatial scales would substantially benefit the VPM model and other models that estimate GPP of terrestrial ecosystems. The second source is the systematic error of tower-based GPP_{obs}. The value of GPP_{obs} is calculated as the difference between R_e (observed nighttime NEE and estimated daytime ecosystem respiration) and flux-measured NEE. For a given value of NEE as measured by the EC method, an error in the estimation of daytime ecosystem respiration would therefore result in an error in the estimation of GPP. Both of these steps require subjective decisions and are currently the subject of a great deal of discussion (Falge et al. 2001, 2002). The third source is the time-series data of vegetation indices derived from satellite images. We used the 8-day MODIS composite images that have no correction or normalization, and thus the effect of angular geometry on surface reflectance and vegetation indices remained. We therefore suggest that future work should focus on measurements of leaf water content, chlorophyll and dry matter during every key phenological transition stage, by that improving our understanding of temporal processes of vegetation indices dynamics (e.g., EVI and LSWI) and in-depth studies on model improvement.

Conclusion

In summary, we demonstrated that temperature was the most important factors controlling CO_2 fluxes in the Zoige alpine wetland ecosystem. Then, we incorporated MODIS EVI and LSWI as well as in situ measurements of climate data into a satellite-based vegetation photosynthesis model to more

adequately quantify ecosystem carbon dynamics. We further tested the model results against GPP datasets measured at the study site. These results indicated that the seasonal dynamics of GPP predicted by the VPM model matched well with observed GPP from eddy flux towers. Satisfied with the validation tests, especially regarding the responses of the modeled GPP fluxes to the climate variation, we will continue validating and developing the modeling approach to explore the potential of the VPM model in alpine wetlands. With further validation and development, the VPM will have the potential to be applied at large spatial scales to estimate GPP in the near future, which will improve our understanding of the carbon cycle of the terrestrial biosphere.

References

Addiscott T, Whitmore A (1987) Computer simulation of changes in soil mineral nitrogen and crop nitrogen during autumn, winter and spring. Journal of Agricultural Science 109:141–157

Asner GP, Clark JK, Mascaro J et al (2012) Human and environmental controls over aboveground carbon storage in Madagascar. Carbon Balance and Management 7:2

Baldocchi DD (2003) Assessing the eddy covariance technique for evaluating carbon dioxide exchange rates of ecosystems: past, present and future. Global Change Biology 9:479–492

Baldocchi D, Falge E, Gu LH et al (2001) FLUXNET: a new tool to study the temporal and spatial variability of ecosystem-scale carbon dioxide, water vapor, and energy flux densities. Bulletin of the American Meteorological Society 82:2415–2434

Belshe E, Schuur E, Bolker B, Bracho R (2012) Incorporating spatial heterogeneity created by permafrost thaw into a landscape carbon estimate. Journal of Geophysical Research 117, G01026

Chen J, Saunders S, Brosofske K, Crow T (2006) Ecology of hierarchical landscapes: from theory to application. Nova Science Publisher, New York

Chen H, Yao S, Wu N et al (2008) Determinants influencing seasonal variations of methane emissions from alpine wetlands in Zoige Plateau and their implications. Journal of Geophysical Research 113, D12303

Chen H, Wu N, Gao YH, Wang YF, Luo P, Tian JQ (2009) Spatial variations on methane emissions from Zoige alpine wetlands of Southwest China. Science of the Total Environment 407:1097–1104

Chen H, Wu N, Wang YF et al (2013) Inter-annual variations of methane emission from an open fen on the Qinghai-Tibetan Plateau: a three-year study. PLoS ONE 8:e53878

Elmendorf SC, Henry GHR, Hollister RD et al (2012) Global assessment of experimental climate warming on tundra vegetation: heterogeneity over space and time. Ecology Letters 15:164–175

Erwin KL (2009) Wetlands and global climate change: the role of wetland restoration in a changing world. Wetlands Ecology and Management 17:71–84

Falge E, Baldocchi D, Olson R et al (2001) Gap filling strategies for defensible annual sums of net ecosystem exchange. Agricultural and Forest Meteorology 107:43–69

Falge E, Baldocchi D, Tenhunen J et al (2002) Seasonality of ecosystem respiration and gross primary production as derived from FLUXNET measurements. Agricultural and Forest Meteorology 113:53–74

Friedlingstein P, Cox P, Betts R et al (2006) Climate-carbon cycle feedback analysis: results from the C4MIP model intercomparison. Journal of Climate 19:3337–3353

Goetz SJ, Prince SD, Goward SN, Thawley MM, Small J (1999) Satellite remote sensing of primary production: an improved production efficiency modeling approach. Ecological Modelling 122:239–255

Goulden ML, Munger JW, Fan SM, Daube BC, Wofsy SC (1996) Measurements of carbon sequestration by long-term eddy covariance: methods and a critical evaluation of accuracy. Global Change Biology 2:169–182

Guindin-Garcia N, Gitelson AA, Arkebauer TJ, Shanahan J, Weiss A (2012) An evaluation of MODIS 8-and 16-day composite products for monitoring maize green leaf area index. Agricultural and Forest Meteorology 161:15–25

Hao Y, Wang Y, Mei X, Cui X, Zhou X, Huang X (2010) The sensitivity of temperate steppe CO_2 exchange to the quantity and timing of natural interannual rainfall. Ecological Informatics 5:222–228

Hao YB, Cui XY, Wang YF et al (2011) Predominance of precipitation and temperature controls on ecosystem CO_2 exchange in Zoige alpine wetlands of Southwest China. Wetlands 31:413–422

Hao YB, Kang XM, Wu X et al (2013) Is frequency or amount of precipitation more important in controlling CO_2 fluxes in the 30-year-old fenced and the moderately grazed temperate steppe? Agriculture, Ecosystems and Environment 171:63–71

Hashimoto H, Wang W, Milesi C et al (2012) Exploring simple algorithms for estimating gross primary production in forested areas from satellite data. Remote Sensing 4:303–326

Houborg RM, Soegaard H (2004) Regional simulation of ecosystem CO_2 and water vapor exchange for agricultural land using NOAA AVHRR and Terra MODIS satellite data. Application to Zealand, Denmark. Remote Sensing of Environment 93:150–167

Huang Y, Yu YQ, Zhang W et al (2009) Agro-C: a biogeophysical model for simulating the carbon budget of agroecosystems. Agricultural and Forest Meteorology 149:106–129

Huete AR, Liu HQ, Batchily K, van Leeuwen W (1997) A comparison of vegetation indices over a global set of TM images for EOS-MODIS. Remote Sensing of Environment 59:440–451

Huntingford C, Lowe J, Booth B, Jones C, Harris G, Gohar L, Meir P (2009) Contributions of carbon cycle uncertainty to future climate projection spread. Tellus B 61:355–360

Huxman T, Turnipseed A, Sparks J, Harley P, Monson R (2003) Temperature as a control over ecosystem CO_2 fluxes in a high-elevation, subalpine forest. Oecologia 134:537–546

Inglett KS, Inglett PW, Reddy KR, Osborne TZ (2012) Temperature sensitivity of greenhouse gas production in wetland soils of different vegetation. Biogeochemistry 108:77–90

Janssen PHM, Heuberger PSC (1995) Calibration of process-oriented models. Ecological Modelling 83:55–66

Kang X, Hao Y, Li C et al (2011) Modeling impacts of climate change on carbon dynamics in a steppe ecosystem in Inner Mongolia, China. Journal of Soils and Sediments 11:562–576

Kang XM, Hao YB, Cui XY et al (2013) Effects of grazing on CO_2 balance in a semiarid steppe: field observations and modeling. Journal of Soils and Sediments 13:1012–1023

Kayastha N, Thomas V, Galbraith J, Banskota A (2012) Monitoring wetland change using inter-annual landsat time-series data. Wetlands 32:1149–1162

Klein JA, Harte J, Zhao XQ (2007) Experimental warming, not grazing, decreases rangeland quality on the Tibetan Plateau. Ecological Applications 17:541–557

Kljun N, Calanca P, Rotachhi MW, Schmid HP (2004) A simple parameterisation for flux footprint predictions. Boundary-Layer Meteorology 112:503–523

Law BE, Falge E, Gu L et al (2002) Environmental controls over carbon dioxide and water vapor exchange of terrestrial vegetation. Agricultural and Forest Meteorology 113:97–120

Leuning R, Cleugh HA, Zegelin SJ, Hughes D (2005) Carbon and water fluxes over a temperate Eucalyptus forest and a tropical wet/dry savanna in Australia: measurements and comparison with MODIS remote sensing estimates. Agricultural and Forest Meteorology 129:151–173

Li Z, Yu G, Xiao X et al (2007) Modeling gross primary production of alpine ecosystems in the Tibetan Plateau using MODIS images and climate data. Remote Sensing of Environment 107:510–519

Liu J, Chen S, Han X (2012) Modeling gross primary production of two steppes in Northern China using MODIS time series and climate data. Procedia Environmental Sciences 13:742–754

Malhi Y (2012) The productivity, metabolism and carbon cycle of tropical forest vegetation. Journal of Ecology 100:65–75

Matías L, Castro J, Zamora R (2012) Effect of simulated climate change on soil respiration in a Mediterranean-type ecosystem: rainfall and habitat type are more important than temperature or the soil carbon pool. Ecosystems 15:299–1310

Mitsch WJ, Bernal B, Nahlik AM et al (2012) Wetlands, carbon, and climate change. Landscape Ecology 28:583–597

Mu Q, Heinsch FA, Zhao M, Running SW (2007) Development of a global evapotranspiration algorithm based on MODIS and global meteorology data. Remote Sensing of Environment 111:519–536

Oechel WC, Vourlitis GL, Hastings SJ, Zulueta RC, Hinzman L, Kane D (2000) Acclimation of ecosystem CO_2 exchange in the Alaskan Arctic in response to decadal climate warming. Nature 406:978–981

Post E, Pedersen C (2008) Opposing plant community responses to warming with and without herbivores. Proceedings of the National Academy of Sciences 105:12353–12358

Rotenberg E, Yakir D (2010) Contribution of semi-arid forests to the climate system. Science 327:451

Running S, Baldocchi D, Turner D, Gower S, Bakwin P, Hibbard K (1999) A global terrestrial monitoring network integrating tower fluxes, flask sampling, ecosystem modeling and EOS satellite data. Remote Sensing of Environment 70:108–127

Rustad L, Campbell J, Marion G et al (2001) A meta-analysis of the response of soil respiration, net nitrogen mineralization, and aboveground plant growth to experimental ecosystem warming. Oecologia 126:543–562

Saito M, Kato T, Tang Y (2008) Temperature controls ecosystem CO_2 exchange of an alpine meadow on the northeastern Tibetan Plateau. Global Change Biology 15:221–228

Sanderman J, Amundson RG, Baldocchi DD (2003) Application of eddy covariance measurements to the temperature dependence of soil organic matter mean residence time. Global Biogeochemical Cycles 17:1061

Schedlbauer JL, Munyon JW, Oberbauer SF, Gaiser EE, Starr G (2012) Controls on ecosystem carbon dioxide exchange in short-and long-hydroperiod florida everglades freshwater marshes. Wetlands 32:801–812

Smith P, Smith J, Powlson D et al (1997) A comparison of the performance of nine soil organic matter models using datasets from seven long-term experiments. Geoderma 81:153–225

Sulman B, Desai A, Cook B, Saliendra N, Mackay D (2009) Contrasting carbon dioxide fluxes between a drying shrub wetland in Northern Wisconsin, USA, and nearby forests. Biogeosciences 6:1115–1126

Tagesson T, Mastepanov M, Tamstorf MP et al (2012) High-resolution satellite data reveal an increase in peak growing season gross primary production in a high-Arctic wet tundra ecosystem 1992–2008. International Journal of Applied Earth Observation and Geoinformation 18:407–416

Tian Y (2005) The type and distribution of vegetation under different environment in Zoige Alpine wetland. Journal of Yangtze University (Nature Science Edition) 25:1–5

Tucker CJ (1979) Red and photographic infrared linear combinations for monitoring vegetation. Remote Sensing of Environment 8:127–150

Turner DP, Ritts WD, Cohen WB et al (2003) Scaling gross primary production (GPP) over boreal and deciduous forest landscapes in support of MODIS GPP product validation. Remote Sensing of Environment 88:256–270

Walker MD, Wahren CH, Hollister RD et al (2006) Plant community responses to experimental warming across the tundra biome. Proceedings of the National Academy of Sciences of the United States of America 103:1342–1346

Wan S, Hui D, Wallace L, Luo Y (2005) Direct and indirect effects of experimental warming on ecosystem carbon processes in a tallgrass prairie. Global Biogeochemical Cycles 19, GB2014

Wang YF, Cui XY, Hao YB et al (2011) The fluxes of CO_2 from grazed and fenced temperate steppe during two drought years on the Inner Mongolia Plateau, China. Science of the Total Environment 410–411:182–190

Wang SP, Duan JC, Xu GP et al (2012) Effects of warming and grazing on soil N availability, species composition, and ANPP in an alpine meadow. Ecology 93:2365–2376

Wania R, Ross I, Prentice I (2009) Integrating peatlands and permafrost into a dynamic global vegetation model: 2. Evaluation and sensitivity of vegetation and carbon cycle processes. Global Biogeochemical Cycles 23, GB3015. doi:10.1029/2008GB003413

Webb EK, Pearman GI, Leuning R (1980) Correction of flux measurements for density effects due to heat and water-vapor transfer. Quarterly Journal of the Royal Meteorological Society 106:85–100

Wu N (1997) Indigenous knowledge and sustainable approaches for the maintenance of biodiversity in nomadic society. Experiences from the Eastern Tibetan Plateau. Erde-Berlin 128:67–80

Wu WX, Wang SQ, Xiao XM, Yu GR, Fu YL, Hao YB (2008) Modeling gross primary production of a temperate grassland ecosystem in Inner Mongolia, China, using MODIS imagery and climate data. Science in China Series D: Earth Sciences 51:1501–1512

Xiao X, Hollinger D, Aber J, Goltz M, Davidson EA, Zhang Q, Moore B (2004a) Satellite-based modeling of gross primary production in an evergreen needleleaf forest. Remote Sensing of Environment 89:519–534

Xiao X, Zhang Q, Braswell B et al (2004b) Modeling gross primary production of temperate deciduous broadleaf forest using satellite images and climate data. Remote Sensing of Environment 91:256–270

Xiao X, Zhang Q, Hollinger D, Aber J, Moore B (2005a) Modeling gross primary production of an evergreen needleleaf forest using modis and climate data. Ecological Applications 15:954–969

Xiao X, Zhang Q, Saleska S et al (2005b) Satellite-based modeling of gross primary production in a seasonally moist tropical evergreen forest. Remote Sensing of Environment 94:105–122

Xie X, Zhang MQ, Zhao B, Guo HQ (2013) Temperature dependence of coastal wetland ecosystem respiration confounded by tidal activities: a temporal perspective. Biogeosciences Discussions 10:4515–4537

Yan Y, Zhao B, Chen J, Guo H, Gu Y, Wu Q, Li B (2008) Closing the carbon budget of estuarine wetlands with tower-based measurements and MODIS time series. Global Change Biology 14:1690–1702

Yan H, Fu Y, Xiao X, Huang HQ, He H, Ediger L (2009) Modeling gross primary productivity for winter wheat-maize double cropping system using MODIS time series and CO_2 eddy flux tower data. Agriculture, Ecosystems & Environment 129:391–400

Zhang J, Hu Y, Xiao X, Chen P, Han S, Song G, Yu G (2009) Satellite-based estimation of evapotranspiration of an old-growth temperate mixed forest. Agricultural and Forest Meteorology 149:976–984